p14 ARF induces G 2 arrest and apoptosis independently of p53 leading to regression of tumours established into nude mice

Béatrice Eymin, Camille Leduc, Jean-Luc Coll, Elisabeth Brambilla, Sylvie Gazzeri

$p14^{ARF}$ induces G_2 arrest and apoptosis independently of p53 leading to regression of tumours established into nude mice.

Béatrice Eymin, Camille Leduc, Jean-Luc Coll, Elisabeth Brambilla and Sylvie Gazzeri [1].

Groupe de Recherche sur le Cancer du Poumon, EA 2021, Equipe INSERM 9924, Institut Albert Bonniot, 38706 La Tronche Cedex, France

Running title: p53-independent functions of $p14^{ARF}$

Keywords: apoptosis, G_2 arrest, tumour regression, ARF, p53

To whom requests for reprints should be addressed

Sylvie.Gazzeri@ujf-grenoble.fr

Abstract

Until recently, the ability of ARF (human $p14^{ARF}$, murine $p19^{ARF}$) tumour suppressor protein, encoded by the *INK4A/ARF* locus, to inhibit cell growth in response to various stimuli was related to its ability to stabilize p53 through the so-called ARF/MDM2/p53 pathway. However, recent data have demonstrated that ARF is not implicated in this unique p53-dependent pathway. By use of transient and stable expression, we show here that human $p14^{ARF}$ inhibits the growth of human tumoral cells lacking functional p53 by inducing a transient G_2 arrest and subsequently apoptosis. This $p14^{ARF}$-induced G_2 arrest was correlated with inhibition of CDC2 activity, inactivation of CDC25C phosphatase and induction of the CDK inhibitor $p21^{WAF1}$. Apoptosis was demonstrated using Hoechst 33352 staining, proteolytic activation of caspase-3 and PARP cleavage. Similar results were obtained in experiments with cells synchronized by hydroxyurea block. Importantly, we were able to reproduce these effects *"in vivo"* by showing that $p14^{ARF}$ inhibits the growth of p53 nullizygous human tumours in nude mice and induces the regression of p53 -/- established tumours. In these experiments, tumoral regression was associated with inhibition of cell proliferation as well as induction of apoptosis confirming the data obtained in cell lines.

Introduction

The INK4A/ARF locus encodes two structurally distinct proteins, $p16^{INK4a}$ and ARF, translated from alternatively spliced mRNAs (Quelle et al., 1995; Sherr, 1998). Both products are expressed in response to inappropriate proliferative signals and activate pivotal pathways implicated in cell-cycle control and tumour suppression (Chin et al., 1998; Sherr, 1998; Sherr, 2001). The cyclin-dependent kinase inhibitor (CDK-I) $p16^{INK4a}$ prevents phosphorylation and functional inactivation of the retinoblastoma (RB) protein by cyclin-dependent kinases (Serrano et al., 1993). On the other hand, ARF protects against cellular transformation and immortalization by activating the p53 tumour suppressive protein (Sherr, 1998). Expression of ARF is induced in response to activated oncogenes such as Ras (Palmero et al., 1998; Serrano et al., 1997), c-myc (Zindy et al., 1998), E1A (de Stanchina et al., 1998), Abl (Cong et al., 1999; Radfar et al., 1998), and E2F-1 (Bates et al., 1998; Dimri et al., 2000) as well as during replicative senescence (Sherr, 1998). Because ARF-null mice are highly tumour-prone (Kamijo et al., 1997) and die early in life (Kamijo et al., 1999), ARF has been proposed to be most important in tumour surveillance.

Consistent with its role as a tumour suppressor, ARF can induce cell cycle arrest in both G_1 and G_2 phases and/or cell death (Kamijo et al., 1997; Quelle et al., 1995; Stott et al., 1998). Until recently, the growth suppressive function of ARF was related to its ability to stabilize p53 leading to the transcriptional activation of well-known p53-target genes such as $p21^{WAF1}$ or *14.3.3σ* (Weber et al., 2002). However, recent data have pointed to additional p53-independent ARF functions on cell growth but the mechanisms involved remain unclear. In murine systems, $p19^{ARF}$ can suppress colony formation of p53 -/- cells by affecting the RB pathway (Carnero et al., 2000). Furthermore, mice lacking both p53 and $p19^{ARF}$ develop a wilder spectrum of tumours than animals lacking either gene alone, and reintroduction of

p19^{ARF} in mouse embryo fibroblasts (MEF) lacking p53, MDM2 and p19^{ARF} induces cell growth inhibition (Weber et al., 2000). In human, p53-independent ARF activity has been recently ascribed to its ability to impede S-phase progression (Yarbrough et al., 2002) and to induce p53 and Bax-independent apoptosis (Hemmati et al., 2002).

Because we previously showed that human p14^{ARF} can induce growth inhibition of p53-null cells (Eymin et al., 2001), we were interested in better characterizing the pathway(s) involved in the p53-independent functions of p14^{ARF}. To this aim, we transiently or stably expressed p14^{ARF} in human carcinoma cell lines lacking functional p53. Our data show that p14^{ARF} induces a transient G_2 arrest followed by apoptosis in these p53-deprived cells. This G_2 arrest correlates with inhibition of CDC2 activity, inactivation of CDC25C phosphatase, a major upstream regulator of CDC2, and induction of the CDK-I p21^{WAF1}. On the other hand, apoptosis is associated with activation of procaspase-3 and PARP cleavage. Importantly, we also demonstrate that p14^{ARF} inhibits the growth and induces the regression of p53 nullizygous human tumours established in nude mice through inhibition of cell proliferation and induction of apoptosis, demonstrating the *"in vivo"* relevance of our data.

Results

p14^{ARF} induces cell cycle arrest in transiently transfected p53-deficient cells

In order to investigate the p53-independent functions of p14^{ARF}, we transiently transfected two p53-deficient human cell lines derived from bronchioloalveolar lung adenocarcinoma using a full lenght *p14^{ARF}* expression vector. In these cell lines, p53 was inactivated either by homozygous deletion (H358 cells) or single point mutation (H322 cells). In both cell lines, p14^{ARF} strongly inhibited cell growth after 7 days of G418 selection, as a 50% decrease in cell number was observed upon p14^{ARF} transfection as compared to cells

transfected with the empty vector (Figure 1A). In these cells, $p14^{ARF}$ was expressed in the nucleus where it resided predominantly in the nucleoli (Figure 1B). In addition, dual-color flow cytometry revealed that both H358 and H322 cells accumulated with a G_2/M DNA content when transfected with $p14^{ARF}$. Since on visual observation there was no evidence of increased mitotic cells content in this population (data not shown), this pattern is likely to represent a G_2 arrest. Altogether, these results demonstrate the ability of human $p14^{ARF}$ to inhibit cell growth by inducing a G_2 arrest in cells deprived of functional p53.

Inducible $p14^{ARF}$ expression leads to G_2 arrest in stable transfectants clones

In order to confirm the results of transient transfections, we then established stable, $p14^{ARF}$-inducible clones in the H358 cell line using the doxycyclin-inducible expression system (Tet-On). Of note, $p14^{ARF}$ is expressed at a low level in H358 cells (Figure 1A). Several stable transfectant clones were obtained and further analyses were performed on four of them. Since all clones were found to give similar results, representative data of only clones 19 and 38 are presented here. As shown in Figure 2A, a strong expression of $p14^{ARF}$ was detected after 24 hours of doxycyclin induction, which persisted even after 9 days of continuous induction. In contrast, little or no expression of the exogenous $p14^{ARF}$ was observed in the uninduced state (Figure 2A). In these stable inducible clones, expression of $p14^{ARF}$ correlated with its nucleolar accumulation (Figure 2B). As shown in Figure 2C (upper panels), a strong cell growth inhibition was observed upon 9 days of $p14^{ARF}$ induction in both clones. This growth inhibition was significant as early as 72 hours after doxycyclin induction in clone 19 while 6 days were necessary for the clone 38 (Figure 2C, lower panels). Growth inhibition was not detected in an empty tet-on control clone, even in the presence of doxycyclin. Since on the basis of western blot and immunofluorescence analyses, expression of $p14^{ARF}$ was lower in clone 38 than in clone 19 (data not shown), the differences of

inhibition kinetics between clones 19 and 38 was likely related to the different $p14^{ARF}$ expression levels between the two clones. Consistent with these time course studies of cell growth inhibition, a G_2/M arrest was observed following 72 hours of doxycyclin induction in clone 19, and 6 days in clone 38 (Figure 2D). Again, no increase in mitotic cells content was detected in these populations based on visual observation, in agreement with G_2-arrested cells. Interestingly, we noticed the presence of cells with a DNA content greater than 4n upon $p14^{ARF}$ induction (data not shown). Taken together, these results confirm, in stable transfectants clones, the ability of $p14^{ARF}$ to induce a G_2 arrest in a p53-independent manner.

Modulation of cell-cycle protein expression associated with $p14^{ARF}$-induced G_2 arrest

As entry in mitosis is timely controlled by the cyclin B_1/CDC2 complex (Figure 3A; (O'Connell et al., 2000; Takizawa & Morgan, 2000; Weinert, 1997), we analyzed the ability of $p14^{ARF}$ to modulate its activity. Cyclin B_1/CDC2 complexes were recovered by immunoprecipitation using anti-CDC2 antibody and their ability to phosphorylate histone H1 *"in vitro"* was tested in $p14^{ARF}$-induced cells. A strong inhibition of cyclin B_1/CDC2 activity was observed in $p14^{ARF}$-expressing cells as compared to uninduced cells (Figure 3B). Consistent with our cell cycle data (Figure 2D), this inhibition was observed after 72h or 6 days of $p14^{ARF}$ induction, and persisted during 6 or 9 days in clones 19 and 38 respectively (Figure 3B). Under the same conditions, we did not detect any significant change in cyclin B_1 and CDC2 expression levels in $p14^{ARF}$-induced cells immunoblotting when compared to uninduced cells (Figure 3C) and to H358/Tet-On control cells (data not shown).

Before mitosis, cyclin B_1/CDC2 complexes are maintained in an inactive state by phosphorylation of CDC2 on its Thr14 and Tyr15 residues [Figure 3A; (Blasina et al., 1997; Coleman & Dunphy, 1994; Norbury et al., 1991; Ye et al., 1996)]. Dephosphorylation of both

residues causes activation of CDC2 and pushes the cells toward mitosis [(Takizawa & Morgan, 2000), for review]. In addition, full activation of CDC2 also requires the phosphorylation of a conserved threonine residue (Thr161) (Draetta, 1997; Russo et al., 1996). CDC2 phosphorylation status was then examined using specific antibodies recognizing either Tyr15 or Thr161 phosphorylated residues. As a specific phospho-Tyr14 antibody was not available, CDC2-P^{Thr14} status could not be studied. As compared to uninduced cells, a marked decrease of CDC2-P^{Thr161} level was observed in $p14^{ARF}$-expressing cells suggesting that CDC2 was hypophosphorylated on this residue (Figure 3C). In contrast, the same apparent level of CDC2-P^{Tyr15} was detected in both cases (with or without doxycyclin induction ; Figure 3C). As dephosphorylation of CDC2 at tyrosine 15 occurs only in mitotic cells, the level of CDC2-P^{Tyr15} in a population of asynchronous cells, which contains few mitotic cells, is expected to be high. Therefore, we cannot exclude that this could mask an increased level of phosphorylated CDC2 at Tyr15 residue in the population of $p14^{ARF}$-expressing cells principally arrested in G_2. Taken together, these results suggest that $p14^{ARF}$ maintains CDC2 into an inactive state, dephosphorylated at Thr161 residue.

Then, we investigated the status of some upper regulators of the cyclin B_1/CDC2 complexes. At the onset of mitosis, dephosphorylation of both Thr14 and Tyr15 residues on CDC2 is regulated by the CDC25C phosphatase [Figure 3A; (Kumagai & Dunphy, 1991; Millar et al., 1991; Strausfeld et al., 1991)]. CDC25C activity is itself controlled by a complex set of activatory/inhibitory phosphorylations [(Takizawa & Morgan, 2000), for review]. Throughout cell cycle, except in mitosis, CDC25C is maintained inactivated by phosphorylation on its Ser216 residue that creates a binding site for small phosphoserine-binding proteins called 14-3-3 which inactivate CDC25C by sequestration into the cytoplasm (Peng et al., 1997; Takizawa & Morgan, 2000). In $p14^{ARF}$-expressing cells, we detected a slight decrease in CDC25C protein level which was not observed in the H358/Tet-On control

cells in the same conditions (data not shown), as well as an increase of its inactive phosphorylated form at Ser216 (Figure 3C and D). This effect was specific for CDC25C as the level of CDC25B and 14.3.3σ proteins did not appear to vary (data not shown). These data strongly suggest that $p14^{ARF}$ inactivates CDC25C by reducing its total expression level and increasing its inactive phosphorylated form. Furthermore and consistent with a biological inactivation, a cytoplasmic accumulation of CDC2, CDC2-P^{Tyr15} and CDC25C-P^{Ser216} was observed in $p14^{ARF}$-expressing cells (Figure 3E). In contrast, such accumulation never occured in uninduced cells or in H358/Tet-On control cells in agreement with the property of these proteins to shuttle continuously from the cytoplasm to the nucleus of proliferating cells. Finally, as CDC2 activity and phosphorylation status can also be controlled by the $p21^{WAF1}$ CDK-inhibitors family (Dulic et al., 1998; Harper et al., 1995; Niculescu et al., 1998; Smits et al., 2000), expression of some of them was analyzed. An increase of $p21^{WAF1}$ expression level was detected in $p14^{ARF}$-expressing cells (Figure 3C) whereas $p27^{KIP1}$ level remained unchanged (data not shown).

Overall, these results suggest that $p14^{ARF}$ induces a G_2 arrest independently of p53 by preventing the activation of cyclin B_1/CDC2 complexes, at least in part through inactivation of CDC25C phosphatase and induction of $p21^{WAF1}$.

Inhibition of G_2/M phase progression in synchronized $p14^{ARF}$-expressing cells

To confirm the molecular events implicated in the $p14^{ARF}$-induced G_2 arrest, synchronized cells were used. Hydroxyurea (HU) treatment was carried out to block the cells in late G_1 and S phases of the cell cycle, allowing a more precise analysis of cellular DNA content in late stages of the cell cycle after block release, particularly between S and mitosis. In these experiments, $p14^{ARF}$ was induced 24 hours before HU block. As shown in figures 4A and 4B, uninduced control cells accumulated with a G_2/M DNA content until 9 hours after

block release and started to enter mitosis about 13 hours after replating in fresh medium. Twenty four hours after the release, they were predominantly in G_0/G_1 (Figures 4A & 4B). In contrast, and consistent with a G_2/M arrest, a continuous accumulation of $p14^{ARF}$-induced cells in G_2/M phases of the cell cycle was observed between 9 and 13 hours, and persisted even 24 hours (Figures 4A & 4B) and 48 hours (data not shown) after the release. As expected, accumulation of control uninduced cells in G_2/M 13 hours after the block release correlated with a slight upregulation of cyclin B_1 and CDC2 whereas CDC25C protein level did not change (Figure 4C). At this time, and consistent with passage through mitosis, CDC25C was dephosphorylated at Ser216 and CDC2 was activated by dephosphorylation at Tyr15 and phosphorylation at Thr161 residues (Figure 4C). In these control cells, $p21^{WAF1}$ was never induced. In contrast, although $p14^{ARF}$-expressing cells also accumulated with a G_2/M DNA content 13 hours after the block release, CDC2 remained phosphorylated on Tyr15 and hypophosphorylated on Thr161 residues (Figure 4C). These data suggest that CDC2 was in an inactive state in these cells. In addition, concomittant downregulation of CDC25C (Figure 4C and D) and upregulation of inactive CDC25C-P^{Ser216} and of $p21^{WAF1}$ protein expression levels (Figure 4C) were also observed. As this specific pattern of protein expression persisted 24 hours (Figure 4C) and even 48 hours (data not shown) after the block release, these data are in agreement with the absence of passage through mitosis of most of the $p14^{ARF}$-expressing cells. We noticed that a small proportion of cells was still able to overpass this G_2 arrest. This might be linked to the shorter time (24 hours) of $p14^{ARF}$ induction in synchronization experiments compared to those performed on asynchronous cells.

Taken together, these data with synchronized cells confirmed the results obtained in asynchronous $p14^{ARF}$-expressing cells and demonstrate the ability of $p14^{ARF}$ to induce a G_2 arrest independently of p53 by preventing cyclin B_1/CDC2 activation, at least in part through inactivation of CDC25C phosphatase and induction of $p21^{WAF1}$.

G_2 arrest precedes apoptosis in $p14^{ARF}$-expressing cells

Since DNA damage checkpoints may delay cell cycle progression and lead to apoptosis if the cells are unable to undertake repair (Elledge, 1996; Hartwell & Weinert, 1989; Walworth, 2000), we asked whether the $p14^{ARF}$-induced G_2 arrest might ultimately lead to apoptosis in our cells. Using Hoechst 33352 staining, we observed an apoptotic pattern in 20% of the $p14^{ARF}$-expressing cells after 6 or 9 days of doxycyclin induction in clones 19 and 38 respectively. In contrast, this was never detected in uninduced control cells (Figures 5A & 5B), as well as in an inducible control clone, even after 15 days of continuous doxycyclin treatment (data not shown). Under the same conditions, the proteolytic activation of procaspase-3 with appearance of the active p12 and p17 fragments as well as PARP (poly-ADP ribose polymerase) cleavage were specifically observed in $p14^{ARF}$-induced cells (Figure 5C). Apoptosis was confirmed in HU-synchronization experiments, since sub-G_1 DNA content, caspase-3 activation and PARP cleavage were specifically detected in $p14^{ARF}$-expressing cells 48 hours after the block release (Figure 5D). Overall, these results demonstrate that $p14^{ARF}$ is also able to induce apoptosis independently of p53. Moreover, as G_2 arrest was clearly observed before apoptosis could take place (Figures 5A & 5D), our data suggest that G_2 arrest precedes apoptosis in $p14^{ARF}$-expressing cells.

Antitumoral activity of $p14^{ARF}$ in nude mice is associated with cell cycle arrest and apoptosis

In order to determine whether the activity associated with $p14^{ARF}$ expression in cells grown in culture could be reproduced in tumours, H358/Tet-On/$p14^{ARF}$ clones 19 and 38 or H358/Tet-On cells were injected subcutaneously into immunodeficient nude mice. Of note, the growth kinetics of all cells was very similar (data not shown). As identical results were obtained using both clones, representative data of clone 19 are presented here.

We first tested whether the ability of $p14^{ARF}$ to induce G_2 arrest and apoptosis in cell lines might influence the tumoral progression. Whereas the uninduced H358/Tet-On/$p14^{ARF}$ cells (mice drinking water) gave rise to rapid tumour growth, a marked inhibition was observed in mice that received doxycyclin (p=0,0043) (Figure 6A). This effect was specific of $p14^{ARF}$ induction since growth inhibition was not detected in mice injected with H358/Tet-On cells and that received doxycyclin (Figure 6A).

We then asked whether $p14^{ARF}$ was able to prevent the growth of pre-existing tumours lacking p53. H358/Tet-On/$p14^{ARF}$ cells were injected into nude mice and tumours were allowed to grow until they reach 50 to 70 mm^3 volume. At this time, doxycyclin was added or not in their drinking water. A doxycyclin treatment of mice with established H358/Tet-On/$p14^{ARF}$ tumours caused a highly significant tumoral regression after 80 days of treatment (p=0.0043) when compared to mice with same tumours but drinking water only or to mice with established H358/Tet-On tumours and drinking doxycyclin (Figure 6B). This antitumoral activity became statistically significant after 35 days of doxycyclin treatment (p=0.0043). Immunostaining revealed a clear accumulation of $p14^{ARF}$ in H358/Tet-On/$p14^{ARF}$ tumours arising from doxycyclin-treated mice as compared to untreated mice, as well as an inhibition of tumor cell proliferation as determined by KI-67 staining and increased apoptosis as detected by active caspase-3 (Figure 7A) or TUNEL staining (data not shown). When the proliferative index to the apoptotic index was calculated, a lower figure was observed (1.66 versus 4.66) in tumours overexpressing $p14^{ARF}$ than in those with a physiological level of $p14^{ARF}$, in agreement with cell growth inhibition and apoptosis induction. Furthermore, by using western blot analyses on whole tumour extracts, we demonstrated a marked downregulation of total CDC25C which was not detected in the control H358/Tet-On tumours (data not shown) and an apparent stable level of CDC2-P^{Tyr15} (Figure 7B). However, we could not demonstrate any change in CDC25C-P^{Ser216} or $p21^{WAF1}$ protein levels and were unable to

detect CDC2-P^{Thr161} in treated or untreated tumours (data not shown). On the other hand, clear activation of procaspase-3 and PARP cleavage were specifically observed in treated tumours confirming the existence of apoptosis (Figure 7B). Overall, these results demonstrate the ability of $p14^{ARF}$ to inhibit cell growth and to induce apoptosis "*in vivo*".

Discussion

Until recently, the ARF tumour suppressive protein was only ascribed to a well-defined ARF/MDM2/p53 linear pathway. In this model, ARF induces the stabilization and activation of p53 leading to a dual block in G_1 and G_2 phases of the cell cycle and/or cell death (Kamijo et al., 1997; Quelle et al., 1995; Tao & Levine, 1999; Weber et al., 2002; Weber et al., 1999; Zhang & Xiong, 1999). In contrast and despite the existence of many contradictory data, it is now well admitted that ARF also acts onto p53-independent pathways to inhibit cell growth. However, the exact nature of the molecular mechanisms involved in these processes is still unclear and the targets remain unknown. In this study, we demonstrate that $p14^{ARF}$-expressing cells undergo a G_2 arrest in the absence of functional p53 suggesting that p53 might be necessary for G_1 checkpoint but dispensable for G_2 arrest in response to $p14^{ARF}$ induction. Consistently, it was previously reported that p53 -/- cells can accumulate in G_2 following DNA damage (Fan et al., 1995; Li et al., 1995; Lowe et al., 1993; Powell et al., 1995). However, as a prolonged G_2-M arrest requires p53 (Bunz et al., 1998), this could explain why $p14^{ARF}$ induces only a transient G_2 arrest that precedes apoptosis in the absence of active p53. According to our data, the ability of $p14^{ARF}$ to induce p53-independent apoptosis was recently described in p53-deleted SAOS-2 cells and HCT116 p53-/- colon cancer cells (Hemmati et al., 2002). However, cell cycle analysis was not performed in these cells. On the

other hand, Weber et al. recently reported a strict dependency of an intact p53 pathway for $p14^{ARF}$-mediated cell cycle arrest following adenovirus infection (Weber et al., 2002). However, in this last paper, all experiments were performed in a 24-48 hours time frame and no long-term effects were analyzed in contrast to our study. Therefore, as mentionned by the authors, $p14^{ARF}$ might be able to induce arrest or apoptosis in a p53-negative background once activated over a longer time period.

A key step in regulating the entry of eukaryotic cells into mitosis is the activation of the cyclin B_1-CDC2 complex [(Takizawa & Morgan, 2000), for review]. Consistently, a strong inhibition of CDC2 activity was associated with G_2 arrest in $p14^{ARF}$-expressing cells. When we investigated the mechanisms involved in this inhibition, we observed that CDC2 was markedly hypophosphorylated on Thr161 and apparently hyperphosphorylated on Tyr15. The inhibitory phosphorylations on Tyr15 and Thr14 of CDC2 are counteracted by the CDC25C phosphatase (Kumagai & Dunphy, 1991; Millar et al., 1991; Strausfeld et al., 1991). In our $p14^{ARF}$-expressing cells, the level of CDC25C protein was reduced. Total CDC25C protein level is not significantly affected during cell cycle progression (Goldstone et al., 2001) in contrast to its phosphorylation status. Therefore, it is unlikely that the specific decrease of CDC25C level following $p14^{ARF}$ induction could represent the sole consequence of G_2 arrest. Interestingly, as for CDC25A which is downregulated during G_1 checkpoint in response to DNA damage (Mailand et al., 2000), downregulation of CDC25C has been already reported in response to UVB radiations (Athar et al., 2000), γ radiations (Wang et al., 2000) or infection by adenovirus (Raj et al., 2001) and related to a decrease of transcription (Wang et al., 2000) or a degradation by the proteasome complex (Raj et al., 2001). Whether these mechanisms could be implicated in the downregulation of CDC25C protein following $p14^{ARF}$ induction remains to be determined. On the other hand, overexpression and cytoplasmic accumulation of the CDC25C-P^{Ser216} inactive form was observed upon $p14^{ARF}$ induction.

Maintenance of the inhibitory phosphorylation of CDC2 on Thr14/Tyr15 mediated by a CHK-CDC25C pathway has been previously implicated in a G_2 arrest following DNA damage (Peng et al., 1997; Poon et al., 1997; Rhind et al., 1997; Sanchez et al., 1997). In such conditions, inactive phosphorylation of CDC25C on Ser216 by CHK1 and CHK2 kinases was observed, allowing binding to the proteins of the 14.3.3 family and preventing CDC2 activation (Furnari et al., 1997; Graves et al., 2000; Peng et al., 1997; Sanchez et al., 1997). In this way, it would be interesting to study the implication of CHK1 and CHK2 kinases in the $p14^{ARF}$-mediated phosphorylation of CDC25C on Ser216. Overall, although further studies are required to assess the role of CDC25C in $p14^{ARF}$-mediated G_2 arrest, we propose that $p14^{ARF}$ might inactivate CDC25C by both down-regulating its global expression and increasing its inhibitory phosphorylation on Ser216, both mechanisms cooperating to reinforce the G_2 cell cycle checkpoint. Therefore, although we cannot exclude that Tyr15 (and Thr14) phosphorylations of CDC2 could simply be a result rather than a cause of cyclin B_1-CDC2 inactivation linked to multiple feedback loops controlling the activity of $p34^{CDC2}$ complexes (Poon et al., 1997), it is reasonnable to assume that inactivation of CDC25C is implicated in the apparent accumulation of inactive CDC2-P^{Tyr15} upon $p14^{ARF}$ expression.

Concomitantly with CDC25C inactivation, a strong induction of the cyclin-CDK inhibitor $p21^{WAF1}$ was observed in $p14^{ARF}$-expressing cells. Under normal growth conditions, $p21^{WAF1}$ protein accumulates in G_2 (Dulic et al., 1998; Li et al., 1994) and promotes a pause in late G_2 (Dulic et al., 1998). However, several studies have also demonstrated the efficient role of $p21^{WAF1}$ in G_2 checkpoint (Agarwal et al., 1995; Niculescu et al., 1998). Interestingly, Bunz et al. have reported that $p21^{WAF1}$ is essential to sustain rather than to initiate the G_2 checkpoint after DNA damage in human cells (Bunz et al., 1998). Despite its low affinity for the cyclin B_1-CDC2 complexes (Dulic et al., 1998; Harper et al., 1995; Winters et al., 1998), $p21^{WAF1}$ can inhibit CDC2 activity (Yu et al., 1998) and has been recently involved in the inhibition of

its activating phosphorylation on Thr161 (Smits et al., 2000). Whether $p21^{WAF1}$ affects directly or not the phosphorylation status of CDC2 and mediates some of the p53-independent effects of $p14^{ARF}$ remains to be determined. Overall, although we are aware that further studies are required to extend the mechanisms by which $p14^{ARF}$ inhibits cell growth and to clearly identify direct targets, our data suggest that $p14^{ARF}$ induces a G_2 arrest independently of p53 by preventing CDC2 activity through both induction of $p21^{WAF1}$ and inactivation of CDC25C.

Finally and perhaps the most significant aspect of this work was the finding that $p14^{ARF}$ conditional expression inhibits tumour growth and induces the regression of p53-/- human tumours established in nude mice. Importantly, these biological events were associated with an inhibition of cell proliferation as well as an increased apoptosis. Furthermore, although we were unable to reproducibly detect variations in the level of $p21^{WAF1}$ and CDC25C-P^{Ser216}, CDC2, CDC2-P^{Tyr15}, CDC25C, caspase-3 and PARP protein levels varied similarly *"in vitro"* and *"in vivo"* strengthening our data on cell lines. Taken together, our results reinforce the notion that $p14^{ARF}$ can affect pathways and targets other than p53 and demonstrate for the first time that these p53-independent effects can contribute to the tumour suppressive functions of $p14^{ARF}$ *"in vivo"*. They also predicts that loss of $p14^{ARF}$ in tumours that have already inactivated p53, might confer an additive deleterious effect on cell growth. Consistently, Weber et al recently reported that tumours arising in mice lacking ARF and p53 are more aggressive than those in mice lacking either gene alone (Weber et al., 2000). Furthermore, we previously reported the double inactivation of $p14^{ARF}$ and p53 in a large proportion of high grade NE lung tumours (Gazzeri et al., 1998), the most aggressive lung tumours, a concept that received now full agreement in numerous other cancer types (Esteller et al., 2000; Lindstrom et al., 2000; Sanchez-Cespedes et al., 1999). Therefore, reintroduction of $p14^{ARF}$ in these tumours could restore some of the normal checkpoint pathways and thus constitute a major goal of future therapy.

Materials and methods

Cell lines, transfection, proliferation, apoptosis and synchronization assays

H358 and H322 human bronchioloalveolar lung carcinoma cell lines were cultured in RPMI-1640 medium (GIBCO, Cergy Pontoise, France) supplemented with 10% (v/v) heat-inactivated FCS, 2 mM L-glutamine and 100 units/ml penicillin/streptomycin in 5% CO_2 at 37°C. To ensure exponential growth, cells were resuspended in fresh medium 24 hours before transfection. Transient transfections were carried out using FUGENE 6 (Roche Diagnostic) according to the manufacturer's protocol. The total amount of DNA used for transfection was held constant by adding empty control vector. In the growth suppression assay, geneticin (G418; 800 μg/ml) was added to the media 48h post transfection and trypan blue excluding cells were counted one week later. Cell cycle analysis of transient transfection experiments was performed 4 days after same geneticin treatment. For clonogenic assays using $p14^{ARF}$ inducible clones, cells were fixed in 100% ethanol at the indicated times, stained with 1% methylene blue in 0.01 M Borate buffer, pH 8.5 and optical density was measured at 630 nm after elution in HCl 0.1N. Evaluation of apoptosis in stable transfectants clones was carried out after 48h, 72h, 6 days and 9 days of doxycyclin treatment (1 μg/ml) using Hoechst 33352 staining (5 μg/ml, 30 min at 37°C). The percentage of apoptotic cells, identified by their fragmented chromatin, was scored on at least 300 cells using fluorescence microscopy analysis. In the synchronized assays, exponentially H358/Tet-On/$p14^{ARF}$ clones were pretreated during 24 hours with or without 1 μg/ml doxycyclin and further cultured in the presence of 1 mM hydroxyurea (HU) (Sigma). 24 hours after HU treatment, cells were washed twice with PBS and cultured in fresh medium in the presence or absence of doxycyclin for additional indicated times. Cells were then collected and further analyzed for

DNA content and protein expression. Cell-cycle and western blot analyses were processed as described below.

Generation of stable $p14^{ARF}$ inducible clones

Obtention of stable $p14^{ARF}$ inducible clones was performed using a modified tetracyclin-regulated inducible expression system (Tet-On System, Clontech, Ozyme, Saint Quentin en Yvelines, France) according to the manufacturer's protocol. Briefly, H358 cells were transfected in a first round with the pTet-On plasmid which contains the reverse doxycyclin repressor (rtTA) expression cassette, using TFX-50 (Promega, Charbonnières, France) and transferrin (Tfe) (Becton Dickinson, le Pont de Claix, France), and selection of transfectants was performed in the presence of G418 (800 μg/ml). Stable H358/Tet-On clones were screened using the Promega Luciferase Assay System after transient transfections with pTRE-Luc plasmid. A second round of tranfection with pTRE-$p14^{ARF}$ and pTK-Hyg plasmids was then carried out using FUGENE 6. The pTRE-$p14^{ARF}$ plasmid was constructed by subcloning wild-type *$p14^{ARF}$* cDNA downstream of the Tet-regulated promoter into pTRE plasmid. Double transfectants were then selected in the presence of hygromycin (200 μg/ml) and geneticin (100 μg/ml), and screened for $p14^{ARF}$ expression by western blotting following 48 hours of doxycyclin induction (1 μg/ml). Four clones were arbitrarily selected for further experiments.

Antibodies

Monoclonal antibodies (mAbs) used included anti-CDC2/CDK1 (Ab-3, Oncogene Research), anti-CDC2 p34 (sc-54, Santa-Cruz, TEBU, Le Perray-en-Yvelines), anti-CDC25C (67211A, Pharmingen), anti-phospho-CDC25C (Ser216) (9D1, Cell Signaling), anti-cyclin B_1 (14541A, Pharmingen), anti-human KI67 antigen (clone Ki-67, DAKO) and anti-$p21^{WAF1}$

(Ab-1, clone EA10, Oncogene Research). Polyclonal antibodies used included anti-actin (20-33, Sigma, Saint Quentin Fallavier, France), anti-caspase-3 (65906E, Pharmingen), anti-human caspase-3 active (R&D System), anti-phospho-CDC2 (Tyr15) (Cell Signaling), anti-phospho-CDC2 (Thr161) (Cell Signaling), anti $p14^{ARF}$ (Ab-1, Oncogene Research) and anti-PARP (Roche Diagnostics).

Cell-cycle analysis

Cells were washed twice in PBS and fixed in ice-cold acetone for 5 min at –20°C. After two PBS washes, cells were saturated with 2% BSA, 2% goat serum in PBS for 30 min at room temperature and incubated overnight at +4°C with gentle rotation in presence of anti-$p14^{ARF}$ (Ab-1, 1/200). After extended washes in PBS, Alexa™ 488 goat anti-rabbit-IgG (H+L) conjugate (2 mg/ml; 1/500, Interchim, Montluçon) was added for 30 min at room temperature. Cells were then washed twice in PBS, incubated at 37°C for 30 min with 200 U/ml of RNAse A (Sigma) and then with propidium iodide (10 μg/ml in PBS). Cell-cycle distribution of $p14^{ARF}$-expressing cells was determined by dual-color flow cytometry using the Cellfit software (Becton Dickinson, Grenoble, France).

Indirect immunofluorescence

$50x10^3$ cells/well were seeded onto 4-wells LAB-TEK®. At indicated times, cells were fixed in 4% paraformaldehyde for 5 min at room temperature (RT), washed three times, saturated in presence of 2% BSA, 2% goat serum in PBS for 30 min at RT and further incubated with anti-$p14^{ARF}$ (Ab-1, Oncogene Research; 1/1000) for 2 hours. After three PBS washes, Alexa™ 488 goat anti-rabbit IgG (H+L) conjugate (2 mg/ml; 1/500, Interchim, Montluçon) was added for 30 min at RT and the cells were then whashed twice in PBS.

Normal rabbit IgG at the same concentration as the primary antibody served as a negative control. Cells were counterstained with Hoechst and observed using an Olympus microscope (20x magnification). Images were captured with a Coolview CCD camera (Photonic Science) and digitally saved using Visilog software.

Immunoblotting

Cells or frozen tumour tissues were lysed in RIPA buffer for 30 min on ice, pelleted and the protein concentration was determined using the Biorad Dc protein assay. 20-40 μg protein were then separated by SDS-PAGE in 7-12% gels and electroblotted onto PVDF membranes (Amersham Pharmacia, France). Membranes were incubated overnight at +4°C with primary antibody and proteins were detected using horseradish peroxidase-conjugated goat anti-mouse or anti-rabbit antibodies (Jackson ImmunoResearch Laboratories, West Grove, PA) and enhanced chemiluminescence detection system (Amersham, Les Ulis, france). To confirm the slight variation of CDC25C expression level, immunoblots were analyzed by densitometry using the NIH 1.6 software. Further quantification was performed by normalizing the signals with respect to that of the actin loading control. Results were expressed as a CDC25C/actin ratio which was arbitrarily normalized to a 100% expression level in uninduced cells at each time studied.

For cytoplasmic extracts, cells were incubated for 30 min into an ice-cold buffer containing 250 mM Sucrose, 20 mM HEPES-KOH, pH 7.5, 1.5 mM $MgCl_2$, 1 mM EDTA, 1 mM EGTA, 1 mM DTT and protease/phosphatase inhibitors. Permeabilization was carried out by serial passages of the cell suspension through a 25G seringue until the obtention of 70-80% trypan blue positive cells. Centrifugation at 1700 rpm was then performed for 5 min and supernatants were ultracentrifugated for 30 min at 55.000 rpm in order to obtain the cytosolic fraction.

"In vitro" kinase reaction

Cells were washed three times with PBS, resuspended in lysis buffer (150 mM NaCl, 1mM EDTA, 1 mM EGTA, 50 mM Tris-HCl pH 7.4, 1% Triton 100X, 0.2 mM Na_3VO_4, 0.5% Nonidet P40, 0.1 mM PMSF, 2.5 μg/ml pepstatin, 10 μg/ml aprotinin, 5 μg/ml leupeptin), incubated on ice for 30 min and centrifugated for 20 min at 10.000 rpm. Protein concentration was adjusted to 200 μg in 200 μl NET buffer (150 mM NaCl, 50 mM Tris-HCl pH 7.5, 0.1% NP40, 1 mM EDTA pH 8, 0.25% gelatin, 0.02% sodium azide) supplemented with protease inhibitors before use and incubated overnight at +4°C with anti-cyclin B_1 or anti-CDC2 antibodies. 1 mg of protein A/protein G agarose beads was added to each reaction and samples were incubated for 1 hour at + 4°C with gentle rotation. After two washes in NET buffer, beads were subjected to a final wash in kinase buffer (50 mM Tris-HCl, pH 7.6, 10 mM $MgCl_2$, 1 mM DTT). 10 μl aliquots were added to 40 μl of kinase buffer containing 50 μM ATP, 10 μCi (γ-^{32}P) ATP (3000 Ci/mmol) and 50 μg of histone H1 and incubated 30 min at 30°C. Samples were boiled in the presence of 50 μl SDS-PAGE loading buffer and subjected to electrophoresis on a 12% polyacrylamide gel. CDC2 activity was visualized by autoradiography.

Tumour treatment

"In vivo" experiments were conducted onto six-weeks-old female Swiss nude mice (Iffa Credo, Marcy l'Etoile, France). In all experiments, $20x10^6$ H358/Tet-On/$p14^{ARF}$ cells were injected subcutaneously into the nude mice and randomized into two groups, one receiving doxycyclin (2 mg/ml) in their drinking water and the second one receiving water only. An additional group of nude mice injected with $20x10^6$ H358/Tet-On cells and treated with doxycyclin was used as control. The tumour volumes were measured once a week in two perpendicular diameters and calculated as follows: a x b^2 x 0.4, where "a" and "b" are the

largest and smallest diameters, respectively. All experiments were repeated twice for both 19 and 38 clones. In the tumour uptake assay, doxycyclin was provided immediately after cells injection. Each group was composed of 8 animals and difference in tumour volume was assessed using a non parametric Mann-Whitney t test. Study of tumour regression was performed on 10 animals per group that received doxycyclin or water when tumour volumes ranged from 50 to 70 mm^3 (about two or three weeks later). Mice were sacrified at differents times and tumours were divided into two parts before frozing in order to perform western blotting or immunohistochemistry. Statistical analysis between the tumour volumes of the different groups was performed using a non parametric Mann-Whitney t test on 6 animals per group.

Immunohistochemical staining

Immunostaining of $p14^{ARF}$, active caspase-3 and KI67 was performed on frozen sections, as previously described for $p14^{ARF}$ and KI67 (Gazzeri et al., 1998; Labat-Moleur et al., 1998) and according to the manufacturer's protocol for caspase-3. Briefly, three step immunohistochemical method was applied on 5 μM thick frozen sections. After fixation, non specific binding sites were blocked by incubating the sections with 0.1% (w/v) BSA in phosphate-buffered saline (PBS) for 30 minutes at room temperature. The sections were subsequently incubated with primary antibodies overnight at 4°C, washed in PBS several times and exposed to biotinylated secondary antibodies consisting of either anti-rabbit biotinylated donkey F(ab')2 (1/1000; The Jackson Laboratory; West Grove; PA) or anti-mouse biotinylated donkey F(ab')2 (1/500; The Jackson Laboratory) for 1 hour at room temperature. Slides were then washed in PBS and incubated with the streptavidin-biotin-peroxydase complex (1/200; Strept-AB complex; DAKO) for 1 hour at room temperature.

The slides were counterstained with Harris' hematoxylin. Normal rabbit or mouse IgG at the same concentration as the primary antibodies served as negative controls.

Acknowledgements

This work was supported by a grant to E.B. from La Ligue Nationale Contre le Cancer as an « équipe labellisée » and by the Association pour la Recherche sur le Cancer. B.E. was supported by INSERM (Poste Accueil). We thank Christiane Oddou, Pascal Perron, Christine Claraz and Sylvie Veyrenc for technical assistance.

References

Agarwal, M.L., Agarwal, A., Taylor, W.R. & Stark, G.R. (1995). *Proc Natl Acad Sci U S A*, **92,** 8493-7.

Athar, M., Kim, A.L., Ahmad, N., Mukhtar, H., Gautier, J. & Bickers, D.R. (2000). *Biochem Biophys Res Commun*, **277,** 107-11.

Bates, S., Phillips, A.C., Clark, P.A., Stott, F., Peters, G., Ludwig, R.L. & Vousden, K.H. (1998). *Nature*, **395,** 124-5.

Blasina, A., Paegle, E.S. & McGowan, C.H. (1997). *Mol Biol Cell*, **8,** 1013-23.

Bunz, F., Dutriaux, A., Lengauer, C., Waldman, T., Zhou, S., Brown, J.P., Sedivy, J.M., Kinzler, K.W. & Vogelstein, B. (1998). *Science*, **282,** 1497-501.

Carnero, A., Hudson, J.D., Price, C.M. & Beach, D.H. (2000). *Nat Cell Biol*, **2,** 148-55.

Chin, L., Pomerantz, J. & DePinho, R.A. (1998). *Trends Biochem Sci*, **23,** 291-6.

Coleman, T.R. & Dunphy, W.G. (1994). *Curr Opin Cell Biol*, **6,** 877-82.

Cong, F., Zou, X., Hinrichs, K., Calame, K. & Goff, S.P. (1999). *Oncogene*, **18,** 7731-9.

de Stanchina, E., McCurrach, M.E., Zindy, F., Shieh, S.Y., Ferbeyre, G., Samuelson, A.V., Prives, C., Roussel, M.F., Sherr, C.J. & Lowe, S.W. (1998). *Genes Dev*, **12,** 2434-42.

Dimri, G.P., Itahana, K., Acosta, M. & Campisi, J. (2000). *Mol Cell Biol*, **20,** 273-85.

Draetta, G.F. (1997). *Curr Biol*, **7,** R50-2.

Dulic, V., Stein, G.H., Far, D.F. & Reed, S.I. (1998). *Mol Cell Biol*, **18,** 546-57.

Elledge, S.J. (1996). *Science*, **274,** 1664-72.

Esteller, M., Tortola, S., Toyota, M., Capella, G., Peinado, M.A., Baylin, S.B. & Herman, J.G. (2000). *Cancer Res*, **60,** 129-33.

Eymin, B., Karayan, L., Seite, P., Brambilla, C., Brambilla, E., Larsen, C.J. & Gazzeri, S. (2001). *Oncogene*, **10,** 1033-1041.

Fan, S., Smith, M.L., Rivet, D.J., 2nd, Duba, D., Zhan, Q., Kohn, K.W., Fornace, A.J., Jr. & O'Connor, P.M. (1995). *Cancer Res*, **55,** 1649-54.

Furnari, B., Rhind, N. & Russell, P. (1997). *Science*, **277,** 1495-7.

Gazzeri, S., Della Valle, V., Chaussade, L., Brambilla, C., Larsen, C.J. & Brambilla, E. (1998). *Cancer Res*, **58,** 3926-31.

Goldstone, S., Pavey, S., Forrest, A., Sinnamon, J. & Gabrielli, B. (2001). *Oncogene*, **20,** 921-32.

Graves, P.R., Yu, L., Schwarz, J.K., Gales, J., Sausville, E.A., O'Connor, P.M. & Piwnica-Worms, H. (2000). *J Biol Chem*, **275,** 5600-5.

Harper, J.W., Elledge, S.J., Keyomarsi, K., Dynlacht, B., Tsai, L.H., Zhang, P., Dobrowolski, S., Bai, C., Connell-Crowley, L., Swindell, E. & et al. (1995). *Mol Biol Cell*, **6,** 387-400.

Hartwell, L.H. & Weinert, T.A. (1989). *Science*, **246,** 629-34.

Hemmati, P.G., Gillissen, B., von Haefen, C., Wendt, J., Starck, L., Guner, D., Dorken, B. & Daniel, P.T. (2002). *Oncogene*, **21,** 3149-61.

Kamijo, T., Bodner, S., van de Kamp, E., Randle, D.H. & Sherr, C.J. (1999). *Cancer Res*, **59,** 2217-22.

Kamijo, T., Zindy, F., Roussel, M.F., Quelle, D.E., Downing, J.R., Ashmun, R.A., Grosveld, G. & Sherr, C.J. (1997). *Cell*, **91,** 649-59.

Kumagai, A. & Dunphy, W.G. (1991). *Cell*, **64,** 903-14.

Labat-Moleur, F., Guillermet, C., Lorimier, P., Robert, C., Lantuejoul, S., Brambilla, E. & Negoescu, A. (1998). *J Histochem Cytochem*, **46,** 327-34.

Li, C.Y., Nagasawa, H., Dahlberg, W.K. & Little, J.B. (1995). *Oncogene*, **11,** 1885-92.

Li, Y., Jenkins, C.W., Nichols, M.A. & Xiong, Y. (1994). *Oncogene*, **9,** 2261-8.

Lindstrom, M.S., Klangby, U., Inoue, R., Pisa, P., Wiman, K.G. & Asker, C.E. (2000). *Exp Cell Res*, **256,** 400-10.

Lowe, S.W., Schmitt, E.M., Smith, S.W., Osborne, B.A. & Jacks, T. (1993). *Nature*, **362,** 847-9.

Mailand, N., Falck, J., Lukas, C., Syljuasen, R.G., Welcker, M., Bartek, J. & Lukas, J. (2000). *Science*, **288,** 1425-9.

Millar, J.B., Blevitt, J., Gerace, L., Sadhu, K., Featherstone, C. & Russell, P. (1991). *Proc Natl Acad Sci U S A*, **88,** 10500-4.

Niculescu, A.B., 3rd, Chen, X., Smeets, M., Hengst, L., Prives, C. & Reed, S.I. (1998). *Mol Cell Biol*, **18,** 629-43.

Norbury, C., Blow, J. & Nurse, P. (1991). *Embo J*, **10,** 3321-9.

O'Connell, M.J., Walworth, N.C. & Carr, A.M. (2000). *Trends Cell Biol*, **10,** 296-303.

Palmero, I., Pantoja, C. & Serrano, M. (1998). *Nature*, **395,** 125-6.

Peng, C.Y., Graves, P.R., Thoma, R.S., Wu, Z., Shaw, A.S. & Piwnica-Worms, H. (1997). *Science*, **277,** 1501-5.

Poon, R.Y., Chau, M.S., Yamashita, K. & Hunter, T. (1997). *Cancer Res*, **57,** 5168-78.

Powell, S.N., DeFrank, J.S., Connell, P., Eogan, M., Preffer, F., Dombkowski, D., Tang, W. & Friend, S. (1995). *Cancer Res*, **55,** 1643-8.

Quelle, D.E., Zindy, F., Ashmun, R.A. & Sherr, C.J. (1995). *Cell*, **83,** 993-1000.

Radfar, A., Unnikrishnan, I., Lee, H.W., DePinho, R.A. & Rosenberg, N. (1998). *Proc Natl Acad Sci U S A*, **95,** 13194-9.

Raj, K., Ogston, P. & Beard, P. (2001). *Nature*, **412,** 914-7.

Rhind, N., Furnari, B. & Russell, P. (1997). *Genes Dev*, **11,** 504-11.

Russo, A.A., Jeffrey, P.D. & Pavletich, N.P. (1996). *Nat Struct Biol*, **3,** 696-700.

Sanchez, Y., Wong, C., Thoma, R.S., Richman, R., Wu, Z., Piwnica-Worms, H. & Elledge, S.J. (1997). *Science*, **277,** 1497-501.

Sanchez-Cespedes, M., Reed, A.L., Buta, M., Wu, L., Westra, W.H., Herman, J.G., Yang, S.C., Jen, J. & Sidransky, D. (1999). *Oncogene*, **18,** 5843-9.

Serrano, M., Hannon, G.J. & Beach, D. (1993). *Nature*, **366,** 704-7.

Serrano, M., Lin, A.W., McCurrach, M.E., Beach, D. & Lowe, S.W. (1997). *Cell*, **88,** 593-602.

Sherr, C.J. (1998). *Genes Dev*, **12,** 2984-91.

Sherr, C.J. (2001). *Nat Rev Mol Cell Biol*, **2,** 731-7.

Smits, V.A., Klompmaker, R., Vallenius, T., Rijksen, G., Makela, T.P. & Medema, R.H. (2000). *J Biol Chem*, **275,** 30638-43.

Stott, F.J., Bates, S., James, M.C., McConnell, B.B., Starborg, M., Brookes, S., Palmero, I., Ryan, K., Hara, E., Vousden, K.H. & Peters, G. (1998). *Embo J*, **17,** 5001-14.

Strausfeld, U., Labbe, J.C., Fesquet, D., Cavadore, J.C., Picard, A., Sadhu, K., Russell, P. & Doree, M. (1991). *Nature*, **351,** 242-5.

Takizawa, C.G. & Morgan, D.O. (2000). *Curr Opin Cell Biol*, **12,** 658-65.

Tao, W. & Levine, A.J. (1999). *Proc Natl Acad Sci U S A*, **96,** 6937-41.

Walworth, N.C. (2000). *Curr Opin Cell Biol*, **12,** 697-704.

Wang, X., McGowan, C.H., Zhao, M., He, L., Downey, J.S., Fearns, C., Wang, Y., Huang, S. & Han, J. (2000). *Mol Cell Biol*, **20,** 4543-52.

Weber, H.O., Samuel, T., Rauch, P. & Funk, J.O. (2002). *Oncogene*, **21,** 3207-12.

Weber, J.D., Jeffers, J.R., Rehg, J.E., Randle, D.H., Lozano, G., Roussel, M.F., Sherr, C.J. & Zambetti, G.P. (2000). *Genes Dev*, **14,** 2358-65.

Weber, J.D., Taylor, L.J., Roussel, M.F., Sherr, C.J. & Bar-Sagi, D. (1999). *Nat Cell Biol*, **1,** 20-6.

Weinert, T. (1997). *Science*, **277,** 1450-1.

Winters, Z.E., Ongkeko, W.M., Harris, A.L. & Norbury, C.J. (1998). *Oncogene*, **17,** 673-84.

Yarbrough, W.G., Bessho, M., Zanation, A., Bisi, J.E. & Xiong, Y. (2002). *Cancer Res*, **62,** 1171-7.

Ye, X.S., Fincher, R.R., Tang, A., O'Donnell, K. & Osmani, S.A. (1996). *Embo J*, **15,** 3599-610.

Yu, D., Jing, T., Liu, B., Yao, J., Tan, M., McDonnell, T.J. & Hung, M.C. (1998). *Mol Cell*, **2,** 581-91.

Zhang, Y. & Xiong, Y. (1999). *Mol Cell*, **3,** 579-91.

Zindy, F., Eischen, C.M., Randle, D.H., Kamijo, T., Cleveland, J.L., Sherr, C.J. & Roussel, M.F. (1998). *Genes Dev*, **12,** 2424-33.

Legends to figures

Figure 1: p14^{ARF} inhibits cell growth and induces a G_2 arrest in transiently transfected p53-null cell lines.

(A) H322 and H358 cells were transfected with either control pcDNA3.1 (filled bars) or pcDNA-p14^{ARF} (hatched bars). After one week of G418 selection, the remaining adherent cells were counted. In each case, the number of cells transfected with empty vector (control) was normalized to 100%. Results are the means of three independent experiments performed in duplicate. Bars, S.D. Western blot **(A, lower panel)** and immunofluorescence **(B)** analyses of p14^{ARF} expression were performed at the same time. **(C)** Cell cycle analysis was performed on H322 and H358 cells transfected with either control pcDNA3.1 or p14^{ARF} vectors and selected for 4 days with G418. A dual-color flow cytometric analysis was applied after staining of the transfected cells with an anti-p14^{ARF} antibody and cell cycle profile was assessed on the stained population.

Figure 2: Inducible p14^{ARF} expression leads to G_2 arrest in stable transfectants clones.

In all experiments, expression of p14^{ARF} was either uninduced (Dox -) or induced (Dox +) in H358/Tet-On/p14^{ARF} clones 19 and 38 in presence of 1 μg/ml of doxycyclin and experiments were performed at the indicated times. **(A)** Western blotting of p14^{ARF} protein expression in H358/Tet-On/p14^{ARF} clones 19 and 38. **(B)** Nucleolar accumulation of p14^{ARF} in both clones after 72 hours of doxycyclin induction as detected by immunofluorescence. Note the lower level of p14^{ARF} expression in clone 38 as compared to clone 19. **(C)** Inhibition of cell growth by induction of p14^{ARF} expression. Cells were cultured with (Dox +, filled bars) or without (Dox -, empty bars) doxycyclin. Control represents the growth of H358/Tet-On cells containing an empty plasmid. Results are the mean ± SD of three independent experiments.

SD: standard deviation. **(D)** Cell-cycle analysis of the $p14^{ARF}$ positive cells was performed using dual-color flow cytometry. Representative data of at least three independent experiments are shown. Similar results were obtained on the whole cell population after propidium iodide staining (data not shown).

Figure 3: Modulation of proteins regulating the G_2/M transition in $p14^{ARF}$-arrested cells. **(A)** Molecular mechanisms controlling the activation of CDC25C and cyclin B_1/CDC2 at the onset of mitosis. Briefly, in response to proliferative signals, the CDC25C phosphatase is activated by dephosphorylation of its Ser216 residue resulting in its dissociation from 14.3.3 protein and passage into the nucleus. Complete activation of CDC25C also requires extensive phosphorylation of its amino terminus. Following activation, CDC2 is dephosphorylated onto its inhibitory Tyr15 and Thr14 residues by CDC25C and phosphorylated onto its activatory Thr161 residue by the CDK-activating kinase CAK leading to the activation of cyclin B_1/CDC2 complexes. Additional phosphorylations of cyclin B_1 and modifications of the sub-cellular localization of the cyclin B_1/CDC2 complexes also ensure passage into mitosis and have not been represented here. **(B)** CDC2-mediated histone H1 phosphorylation was visualized at the indicated times in both uninduced (Dox -) or induced (Dox +) clones, using an *"in vitro"* kinase assay. **(C)** Pattern of expression of the indicated proteins using western blotting in both clones in the presence (Dox +) or absence (Dox -) of doxycyclin. Actin was used a a loading control. **(D)** Quantification of CDC25C expression level by densitometry in uninduced (DOX-) or induced (DOX+) clones. Results were expressed as a CDC25C/actin ratio which was arbitrarily normalized to a 100% expression level in uninduced cells (DOX-) at each time studied. **(E)** Cytoplasmic expression of CDC2, CDC2-P^{Tyr15} and CDC25C-P^{Ser216} products in uninduced (Dox -) or induced (Dox +) clones using western blotting of a cytoplasmic protein extract.

Figure 4: $p14^{ARF}$ inhibits the G_2/M phase transition in HU-synchronized cells.

H358/Tet-On/$p14^{ARF}$ clone 19 was pretreated during 24 hours with (Dox +) or without (Dox -) 1 μg/ml doxycyclin and further cultured during 24 hours in the presence of 1 mM hydroxyurea (HU). HU block was then released and cells were cultured in fresh medium with (Dox +) or without (Dox -) doxycyclin. Six hours (T6), 9 hours (T9), 13 hours (T13) and 24 hours (T24) after the block release, the cells were collected and processed for dual-color flow cytometry using the Cellfit software (Becton Dickinson) **(A, B)** and western-blot analysis **(C)**. Representative results of three independent experiments are presented. **(D)** Quantification of CDC25C expression level by densitometry in the presence (DOX+) or absence (DOX-) of doxycycline. Analysis was performed as explained in Figure 3D.

Figure 5: $p14^{ARF}$ induces apoptosis independently of p53.

In all experiments, H358/Tet-On/$p14^{ARF}$ clones 19 and 38 were cultured with (Dox +) or without (Dox -) 1 μg/ml of doxycyclin and apoptosis was studied at the indicated times. **(A)** Cells were stained with Hoechst and the percentage of apoptotic cells was scored on at least 300 cells. Results are the mean of three independent experiments ± SD. Bars, SD. G_2/M (%) represents the percentage of cells with a G_2/M DNA content at the same indicated times. **(B)** Apoptotic cells visualized after Hoechst staining and immunofluorescence microscopy. **(C)** Western blot analyses of procaspase-3, active caspase-3 and PARP in both 19 and 38 clones. Actin was used as a loading control. **(D)** Cell cycle profile after dual-color flow cytometry (upper panel) and western blot analyses (lower panel) of procaspase-3, caspase-3 and PARP in HU-synchronized 19 clone. Cells were collected at the time of block release (T0) and 24 hours (T24) or 48 hours (T48) after the block release.

Figure 6: $p14^{ARF}$ inhibits tumour progression and induces tumour regression in nude mice.

Results obtained with the H358/Tet-On/$p14^{ARF}$ clone 19 are presented. **(A)** $p14^{ARF}$ inhibits the growth of tumours. H358/Tet-On/$p14^{ARF}$ cells were sub-cutaneously injected into nude mice and animals were treated with (●) or without (□) 2 mg/ml doxycyclin from the time of injection. Animals injected with H358/Tet-On cells and treated with doxycycline (△) were used as control. At the indicated times, tumour volumes were measured and the mean ± SD was calculated for each group (8 animals per group). **(B)** $p14^{ARF}$ induces regression of pre-existing tumours. H358/Tet-On/$p14^{ARF}$ or H358/Tet-On cells were sub-cutaneously injected into nude mice. Three weeks later, mice bearing detectable tumours from H358/Tet-On/$p14^{ARF}$ cells (50 to 70 mm^3) were randomized into two groups drinking either water (□) or 2 mg/ml doxycyclin (●) whereas mice with H358/Tet-On tumours received doxycycline at the same concentration (△). At the indicated times, tumour volumes were measured and the mean ± SD was calculated for each group (6 animals per group). All experiments were performed twice with similar results. Statistical analyses were performed using a non parametric Mann-Whitney t test. **, $p \leq 0.004$.

Figure 7: $p14^{ARF}$ inhibits cell proliferation and induces apoptosis in nude mice.

H358/Tet-On/$p14^{ARF}$ cells (clone 19) were sub-cutaneously injected into nude mice. After 3 weeks, animals were divided into two groups that received water (Dox -) or 2 mg/ml doxycyclin (Dox +). After 37 days of treatment, mice were sacrified, tumours were collected and further processed for immunostaining **(A)** and western blot **(B)** analyses. **(A)** $p14^{ARF}$, KI67 and active (cleaved) caspase-3 labelling. Notice in treated tumours (Dox +) the strong nuclear staining of $p14^{ARF}$ associated with a nucleolar pattern in 90% of tumour cells, the lower KI67 staining (8.3% versus 14%) reflecting a decrease in cell proliferation and the

higher active caspase-3 (6.4% versus 1.5%) staining reflecting an increased apoptosis as compared to untreated tumours (Dox -). **(B)** Western blotting of $p14^{ARF}$, cyclin B_1, CDC2, CDC2-P^{Tyr15}, CDC25C, caspase-3 and PARP in the same tumour samples. Actin was used as a loading control.

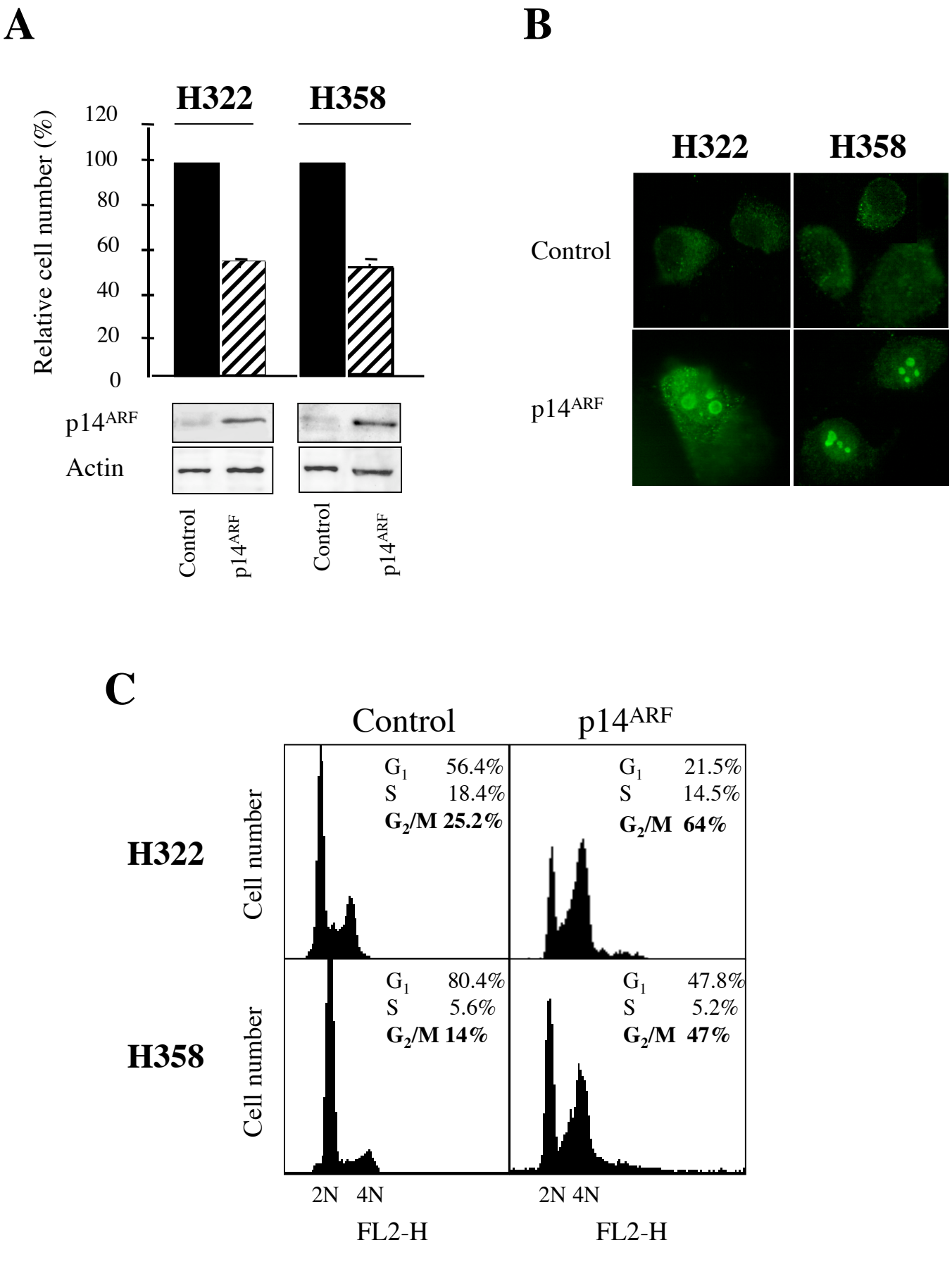
A
H322
H358
Relative cell number (%)
120
100
80
60
40
20
0
p14ARF
Actin
Control
p14ARF
Control
p14ARF
B
H322
H358
Control
p14ARF
C
Control
p14ARF
H322
H358
Cell number
Cell number
G1 56.4%
S 18.4%
G2/M 25.2%
G1 21.5%
S 14.5%
G2/M 64%
G1 80.4%
S 5.6%
G2/M 14%
G1 47.8%
S 5.2%
G2/M 47%
2N 4N
2N 4N
FL2-H
FL2-H

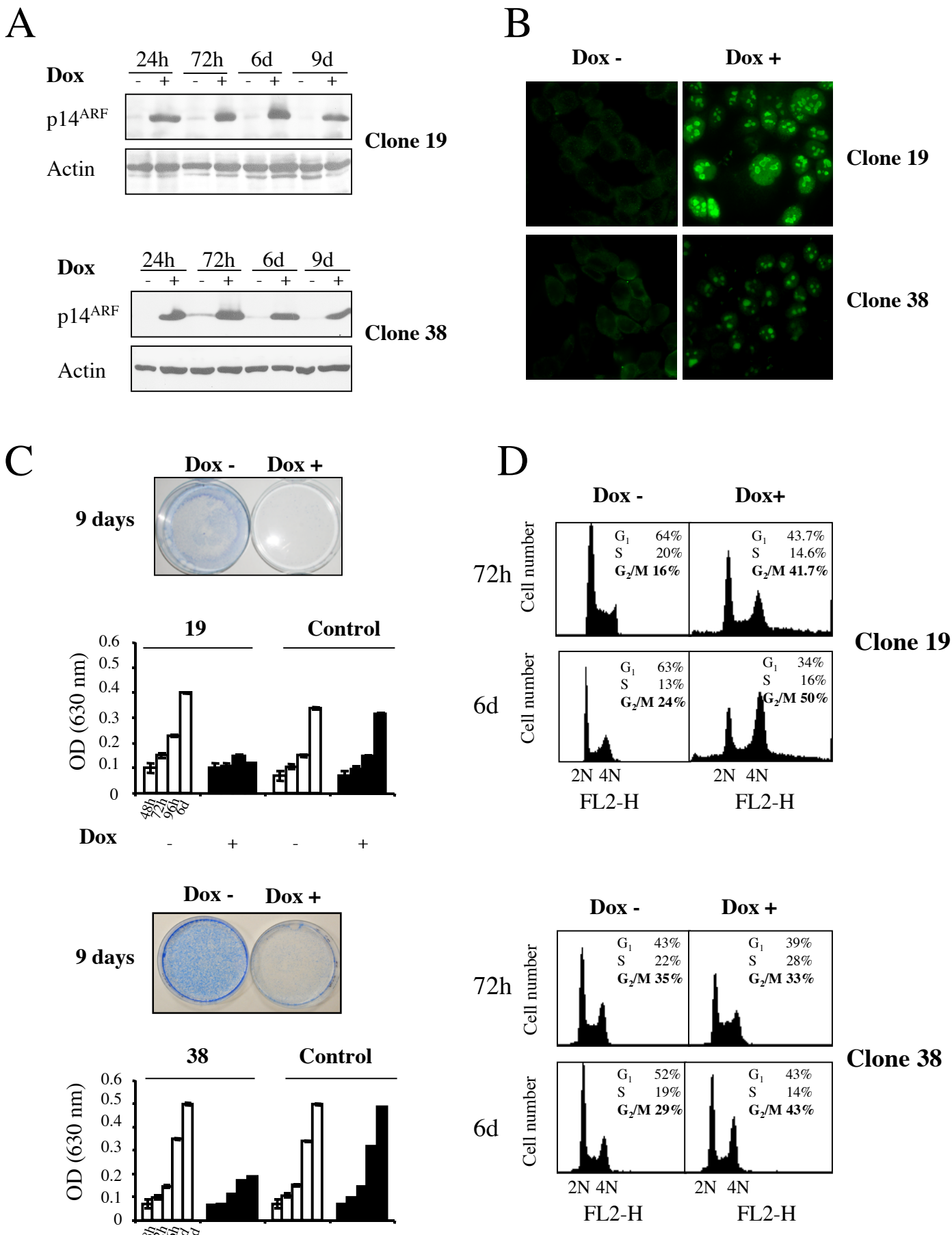
A
Dox
24h
72h
6d
9d
- + - + - + - +
p14ARF
Actin
Clone 19
Clone 38
B
Dox -
Dox +
Clone 19
Clone 38
C
Dox -
Dox +
9 days
19
Control
OD (630 nm)
0.6
0.5
0.4
0.3
0.2
0.1
0
48h
72h
96h
6d
9d
Dox
38
D
Dox -
Dox+
72h
6d
Cell number
G1 64%
S 20%
G2/M 16%
G1 43.7%
S 14.6%
G2/M 41.7%
G1 63%
S 13%
G2/M 24%
G1 34%
S 16%
G2/M 50%
2N 4N
FL2-H
G1 43%
S 22%
G2/M 35%
G1 39%
S 28%
G2/M 33%
G1 52%
S 19%
G2/M 29%
G1 43%
S 14%
G2/M 43%

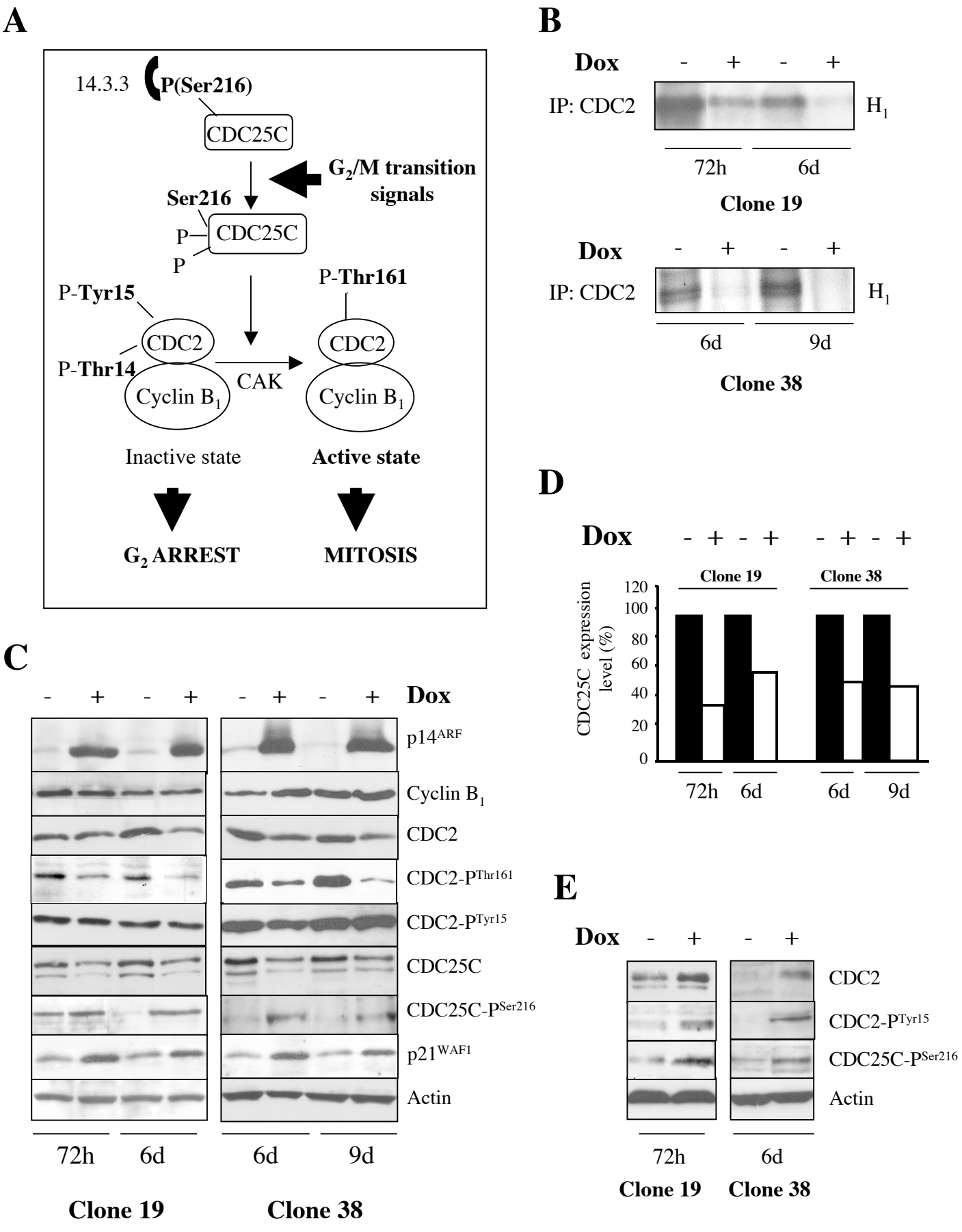
A
14.3.3
P(Ser216)
CDC25C
G2/M transition signals
Ser216
P
CDC25C
P
P-Tyr15
P-Thr161
CDC2
CDC2
P-Thr14
CAK
Cyclin B1
Cyclin B1
Inactive state
Active state
G2 ARREST
MITOSIS
B
Dox - + - +
IP: CDC2
H1
72h 6d
Clone 19
Dox - + - +
IP: CDC2
H1
6d 9d
Clone 38
C
- + - + - + - + Dox
p14ARF
Cyclin B1
CDC2
CDC2-PThr161
CDC2-PTyr15
CDC25C
CDC25C-PSer216
p21WAF1
Actin
72h 6d 6d 9d
Clone 19 Clone 38
D
Dox - + - + - + - +
Clone 19
Clone 38
CDC25C expression level (%)
120
100
80
60
40
20
0
72h 6d 6d 9d
E
Dox - + - +
CDC2
CDC2-PTyr15
CDC25C-PSer216
Actin
72h 6d
Clone 19 Clone 38

A

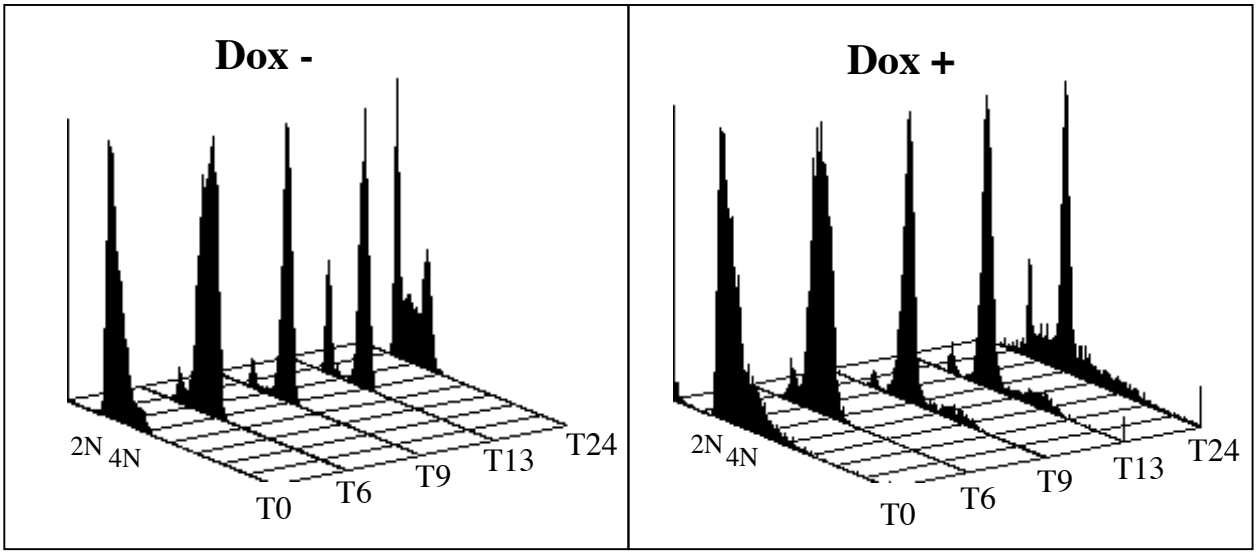

B

	T0		T6		T9		T13		T24	
	Dox -	Dox +	Dox -	Dox +	Dox -	Dox +	Dox -	Dox +	Dox -	Dox +
G_0/G_1 (%)	87.3	75.5	3.1	1.3	4.7	2.4	20.2	3.8	45.9	15.2
S (%)	7.2	17.6	39	50.1	3.3	3.9	1.5	1.02	23.9	11.1
G_2/M (%)	5.5	7	57.9	48.9	92.2	93.7	78.4	95.2	29.7	73.7

C

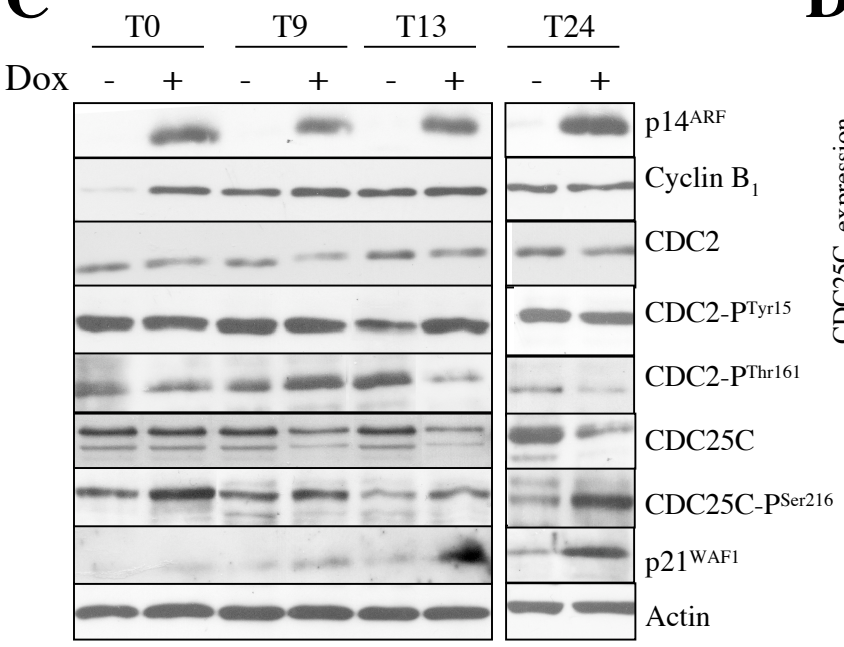

D

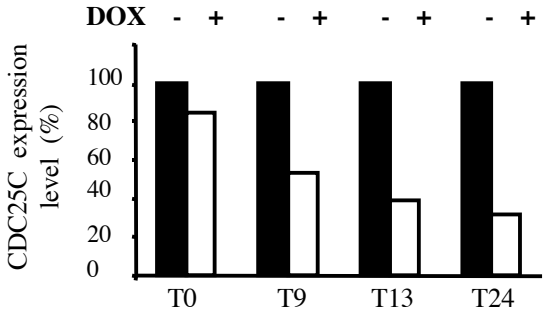

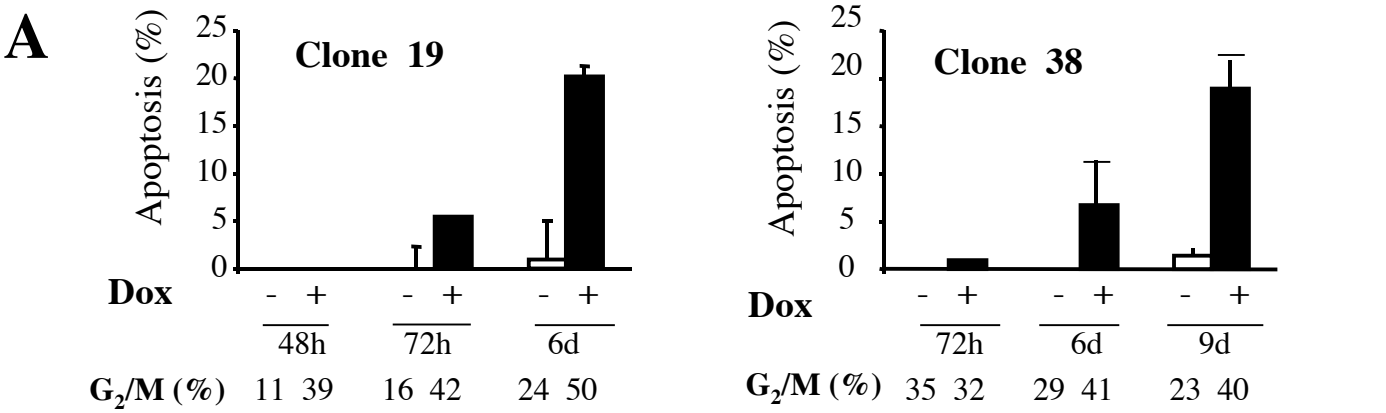
A
Clone 19
Apoptosis (%)
25
20
15
10
5
0
Dox
- + - + - +
48h 72h 6d
G2/M (%) 11 39 16 42 24 50
Clone 38
Apoptosis (%)
25
20
15
10
5
0
Dox
- + - + - +
72h 6d 9d
G2/M (%) 35 32 29 41 23 40

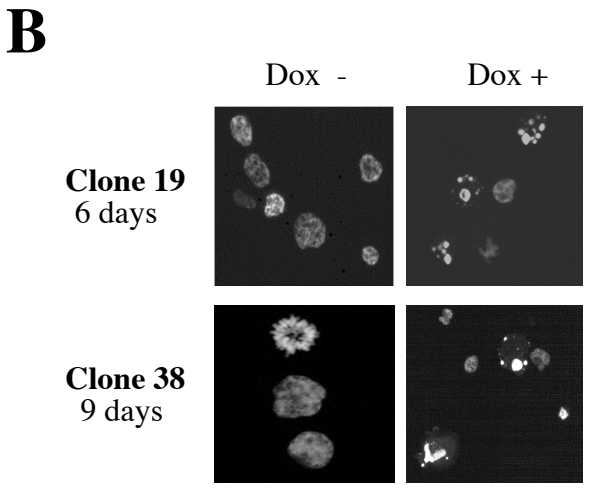
B
Dox -
Dox +
Clone 19
6 days
Clone 38
9 days

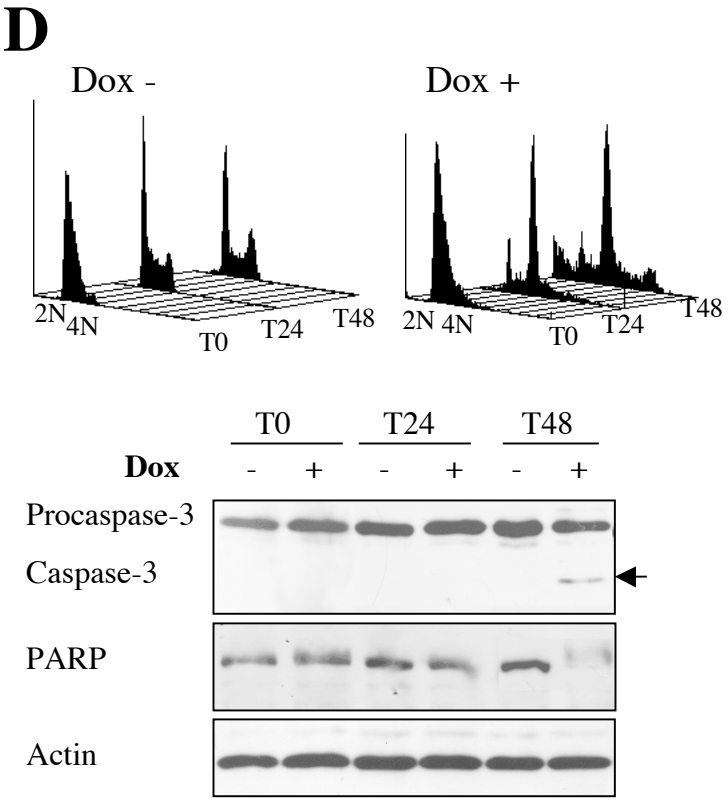
D
Dox -
Dox +
2N 4N
T0
T24
T48
T0 T24 T48
Dox
- + - + - +
Procaspase-3
Caspase-3
PARP
Actin

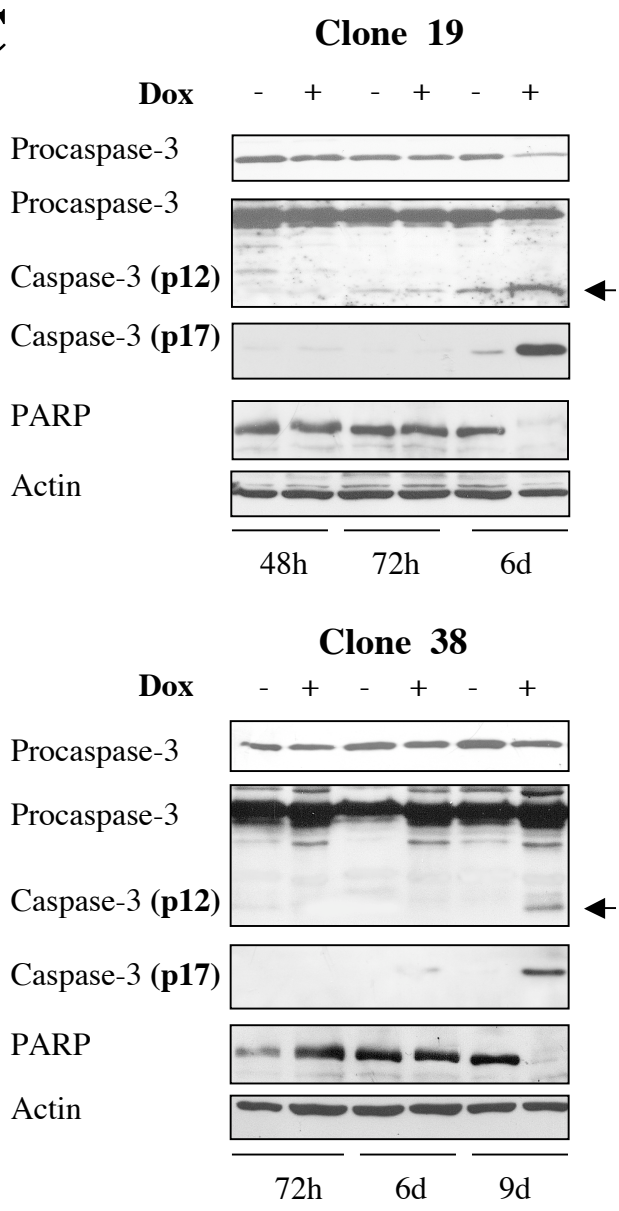
C
Clone 19
Dox
- + - + - +
Procaspase-3
Procaspase-3
Caspase-3 (p12)
Caspase-3 (p17)
PARP
Actin
48h 72h 6d
Clone 38
Dox
- + - + - +
Procaspase-3
Procaspase-3
Caspase-3 (p12)
Caspase-3 (p17)
PARP
Actin
72h 6d 9d

A

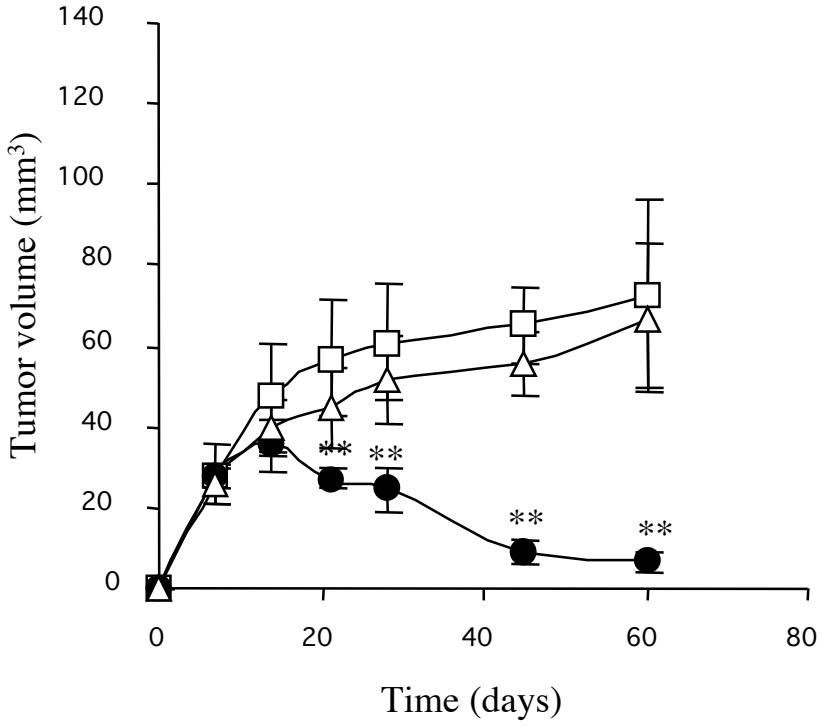
140
120
100
80
60
40
20
0
Tumor volume (mm3)
0
20
40
60
80
Time (days)
**
**
**
**

B

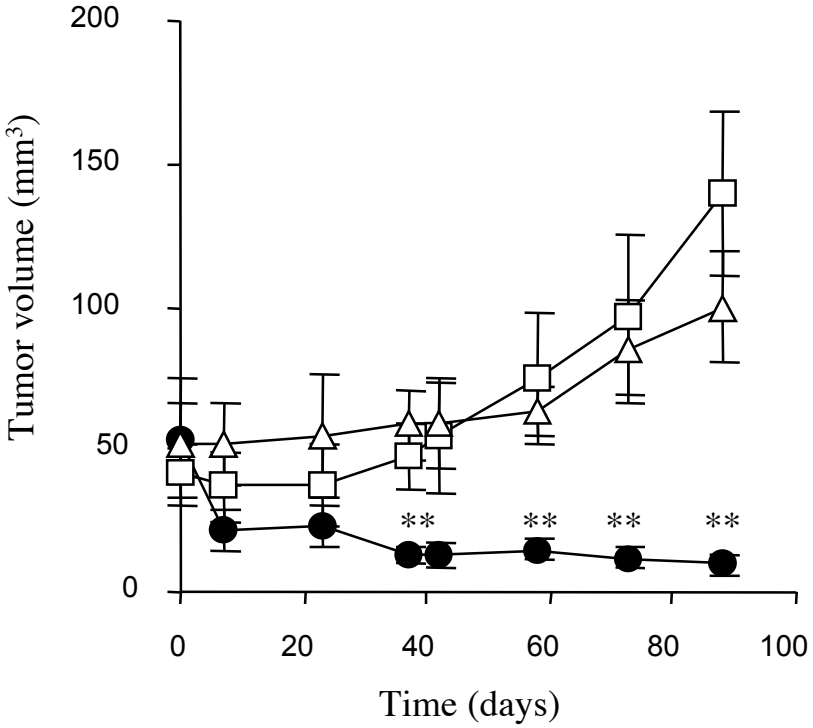
200
150
100
50
0
Tumor volume (mm3)
0
20
40
60
80
100
Time (days)
**
**
**
**

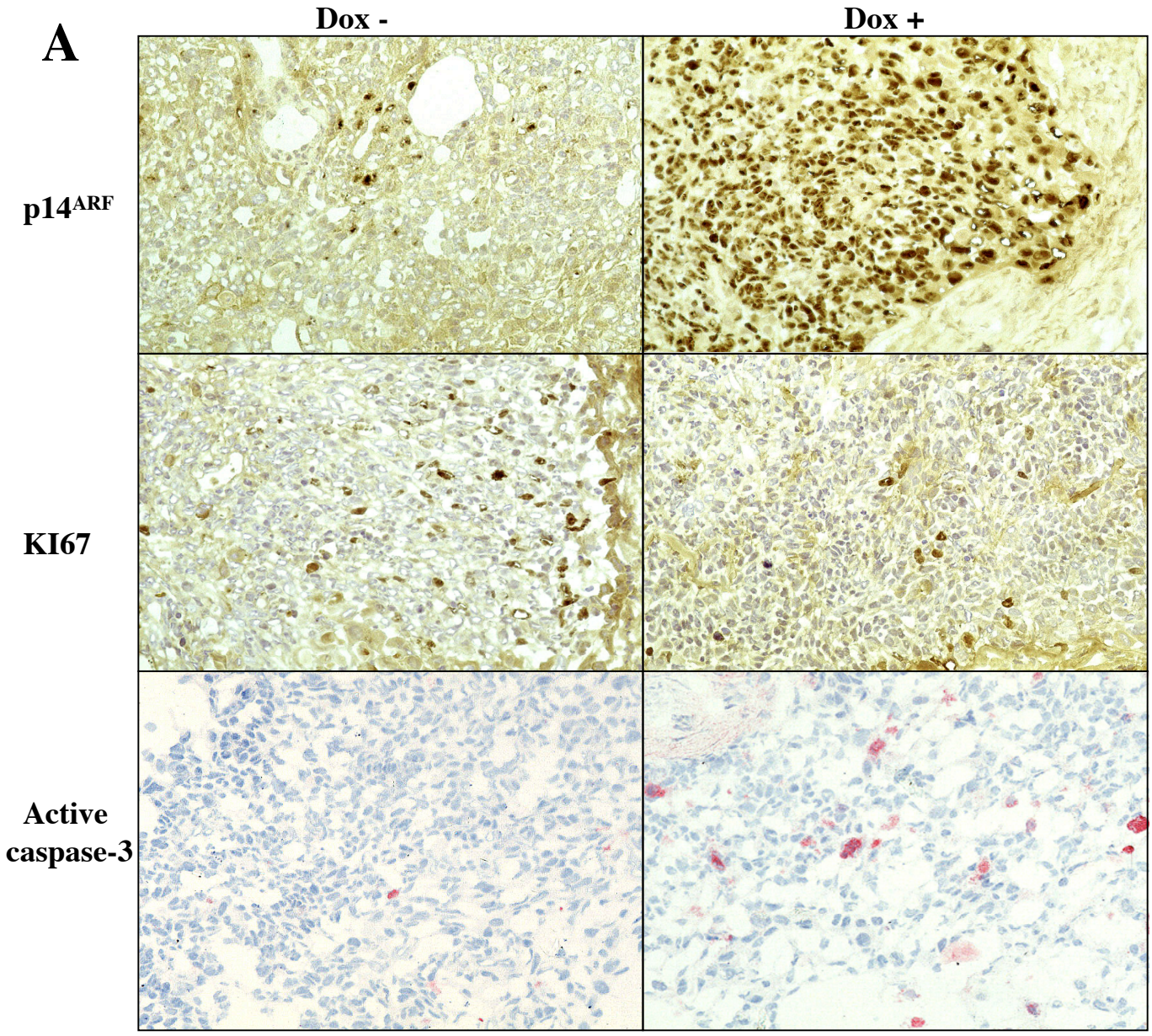
A
Dox -
Dox +
p14ARF
KI67
Active caspase-3
B
Dox - Dox +
p14ARF
Cyclin B1
CDC2
CDC2-PTyr15
CDC25C
Dox - Dox +
Procaspase-3
Caspase-3
Active caspase-3
PARP
Actin